Characterization and Modeling of a Semi-active Rotary Friction Damper

Parker Huggins[1], Liang Cao, Ph.D.[2], Austin R.J. Downey, Ph.D.[1,3], and James Ricles, Ph.D.[2]

[1]Department of Mechanical Engineering, University of South Carolina, Columbia, SC 29208, USA. Email: parkerkh@email.sc.edu

[2]Department of Civil and Environmental Engineering, Lehigh University, Bethlehem, PA 18105, USA.

[3]Department of Civil and Environmental Engineering, University of South Carolina, Columbia, SC 29208, USA.

ABSTRACT

Friction-damping devices are widely accepted as low-cost solutions for enhancing structural resiliency. Of particular interest are semi-active dampers that offer enhanced performance over passive devices while requiring comparatively little input power. A challenge impeding field implementations of friction dampers, however, is the design of robust controllers, particularly for highly nonlinear excitations such as that of an earthquake or wind event. Previously introduced by the authors is a novel semi-active friction damper termed the Banded Rotary Friction Device (BRFD). During operation, the BRFD transduces lateral displacement into angular motion where friction develops as a drum rotates against anchored elastic bands. In this preliminary work, the authors develop a semi-active model for the BRFD whereby damping is controlled via displacement inputs to electric actuators. The model is validated using designed semi-active displacement profiles, and results show that the BRFD lends itself to applications in structural control and natural hazards mitigation.

Keywords: *Variable friction damper (VFD); Semi-active control; Structural control; Natural hazards mitigation; NHERI Lehigh*

INTRODUCTION

The effective reduction of vibration-induced displacements for mechanical and structural systems has long been the subject of much research. Given their frequency-dependent parameters and ability to reliably absorb and dissipate energy, damping devices have emerged as a common solution for mitigating structural vibrations (Saaed et al. 2015). In particular, tuned mass dampers (TMDs) have proved capable of dissipating energy associated with harmonic wind loads and are even installed within select buildings today (Elias and Matsagar 2017). Despite this success, TMDs are curated specifically for a given application and offer damping over a limited bandwidth of excitations, targeting primarily the fundamental frequency of the structure they occupy (Rahimi et al. 2020). While semi-active and active classes of TMDs have been explored to address this shortcoming (Pinkaew and Fujino 2001), research into alternative damping techniques applicable over a wider range of excitations has led to – among other things – the development of the variable friction damper (VFD). Although technically simplistic and cost-effective, VFDs provide competitive damping and overall mechanical robustness (Cao et al. 2016).

Unlike passive friction dampers that are effective only after developed friction surpasses a set slip force, VFDs are semi-active devices with adaptable slip forces altered by the control of a clamping force (Lu 2004). A major advantage of semi-active dampers over active control strategies is that they require the input of comparatively little energy, a resource with potentially limited availability during seismic or sustained wind events (dos Santos 2017). However, serving as a large barrier to VFD implementation is the design of control algorithms consistent with the dynamic behavior of dry friction. Able to describe velocity-dependent characteristics like the Stribeck effect as well as stiction and hysteretic phenomena associated with friction (Johanastrom and Canudas de Wit 2008), the LuGre model was introduced for applications involving the control of dry friction interfaces (Canudas de Wit et al. 1995). Using the LuGre model as a baseline, general semi-active, bang-bang control laws were derived to maximize instantaneous energy dissipation for VFDs (Dupont et al. 1997). Moreover, control schemes exist for a myriad of novel VFDs, including an electromagnetic type (Agrawal and Yang 2004) and a lever arm type (Lu et al. 2018).

In this paper, a semi-active model for a novel rotary friction damper previously proposed by the authors is introduced. Band tension and further damping are controlled via displacement inputs to electric actuators. The organization of the proceeding sections is as follows. First described are the VFD and testbed used for analysis. The relationship between damper output and electric actuator inputs is then developed, and a corresponding semi-active model is proposed. Findings are validated using devised semi-active displacement profiles, and conclusions are drawn from overall model performance and applicability.

BANDED ROTARY FRICTION DEVICE

Furthering on a modified friction damper proposed by the authors (Cao et al. 2015), the Banded Rotary Friction Device (BRFD) was introduced as a semi-active variable friction damper for structural control (Downey et al. 2016). The BRFD consists of a steel drum wound by three elastic bands lined with friction material. During excitation, the drum rotates, and friction develops as contact pressure between the drum and bands increases. In prospective applications, the BRFD serves to do the following: (1) transduce interstory drift – like that experienced by walls of a swaying building – into rotation of the drum; and (2) dissipate energy associated with structural vibrations into heat via friction. For experimentation, the BRFD is connected to a steel foundation beam via bracing elements. A hydraulic actuator provides predefined, lateral displacement profiles. Electric actuators attached to either end of the elastic bands are operated independently and allow for control inputs to the BRFD. By retracting or extending the electric actuators, the force with which the bands clamp onto the drum may be increased or decreased, altering normal force and consequently friction. Load cells are connected to both the hydraulic and electric actuators to measure output damping (friction force) and band tension, respectively. The BRFD and associated testbed for control and data acquisition are displayed in Fig. 1.

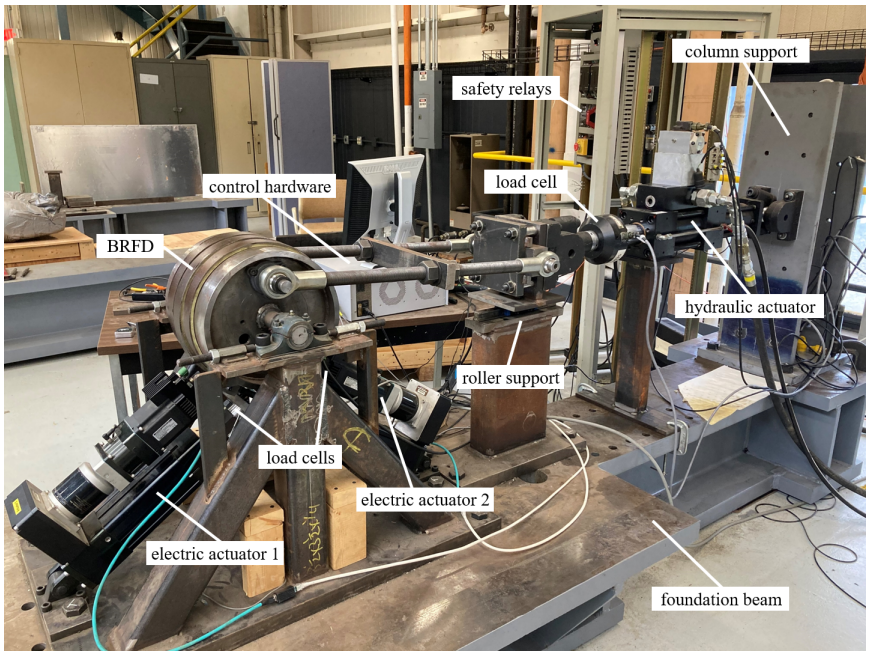

Fig. 1. BRFD and testbed with key components annotated.

Though proposed as a semi-active damper, the BRFD has only been studied and characterized while operating in passive mode. This is in part because the BRFD exhibits a self-energizing effect. As the drum rotates and draws the elastic bands taut, both contact pressure between the drum and bands as well as tension in the bands increase with respect to the point of applied force. This effect stores energy in the system as drum displacement increases but gives it back to the system as displacement decreases. Albeit understood to amplify input and provide sizable damping, in practice the self-energizing effect introduces dynamic asymmetries to the system. For forward rotations of the drum, the band connected to electric actuator two is under tension while the bands connected to electric actuator one are slack. The opposite is true for backward rotations of the drum. This back-and-forth play of forces on the BRFD is illustrated in Fig. 2. As a consequence of such asymmetry, oblique actuator deflections like that pictured in Fig. 3 are induced. Moreover, slight variations in setup conditions vastly affect output; this makes modeling the BRFD in semi-active mode particularly challenging. To date, tests have simply commanded electric actuators to maintain position during excitation.

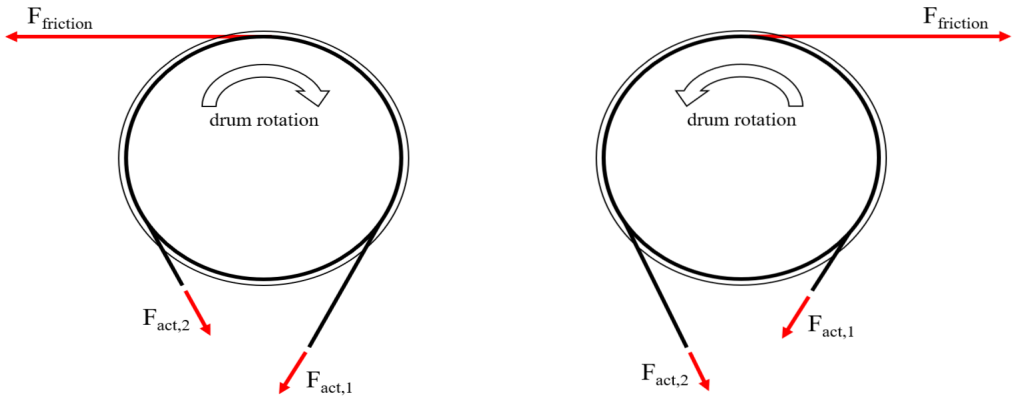

Fig. 2. Schematic of forces acting on the BRFD: (a) forward rotations, $F_{act,2} >> F_{act,1}$; (b) backward rotations, $F_{act,1} >> F_{act,2}$.

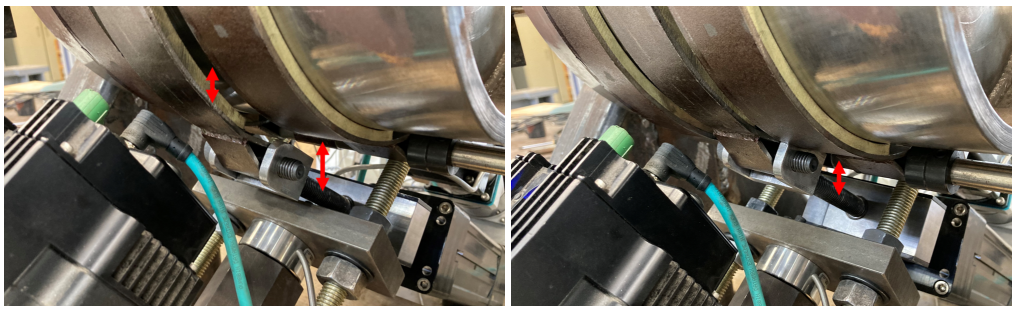

Fig. 3. Electric actuator deflection between (a) slack and (b) taut.

FRICTION MODELING

Much time and effort has been invested into modeling the BRFD in passive mode. Specifically, predicting developed friction for a given displacement profile has been the subject of much analysis. For its ability to capture stick-slip motion, the Stribeck effect, and hysteretic phenomena associated with friction, the LuGre model presented in Eqs. (1-3) has served as a historical baseline for friction characterization of the BRFD. The LuGre model comes in the form of a first-order, nonlinear differential equation with state variable z. The model describes a system of microscopic elastic bristles at the interface of two surfaces in contact. As one surface moves relative to the other, the bristles deflect giving rise to friction.

$$\dot{z} = v - \sigma_0 \frac{|v|}{g(v)} z \tag{1}$$

$$g(v) = F_c + (F_s - F_c) e^{-(v/v_s)^2} \tag{2}$$

$$F = \sigma_0 z + \sigma_1 \dot{z} + \sigma_2 v \tag{3}$$

The model parameters σ_0, σ_1, and σ_2 represent aggregate bristle stiffness, microdamping, and the coefficient of viscous friction, respectively. The function $g(v)$ serves to capture the Stribeck effect whereby increasing velocity between the surfaces in contact (denoted v) evolves friction from a static value, F_s, to a steady state value, F_c, as determined by the Stribeck velocity, v_s. To capture asymmetries associated with developed friction, it is often necessary to consider two sets of F_c and F_s parameters, one for forward rotations and another for backward rotations. That is, use $F_{s,fwd}$ and $F_{c,fwd}$ for $v \geq 0$ but $F_{s,bwd}$ and $F_{c,bwd}$ for $v < 0$. A typical set of hysteresis loops for the BRFD excited by sinusoidal displacement inputs is shown in Fig. 4. The applied force to the BRFD is simply the pretension force existing in the elastic bands prior to excitation.

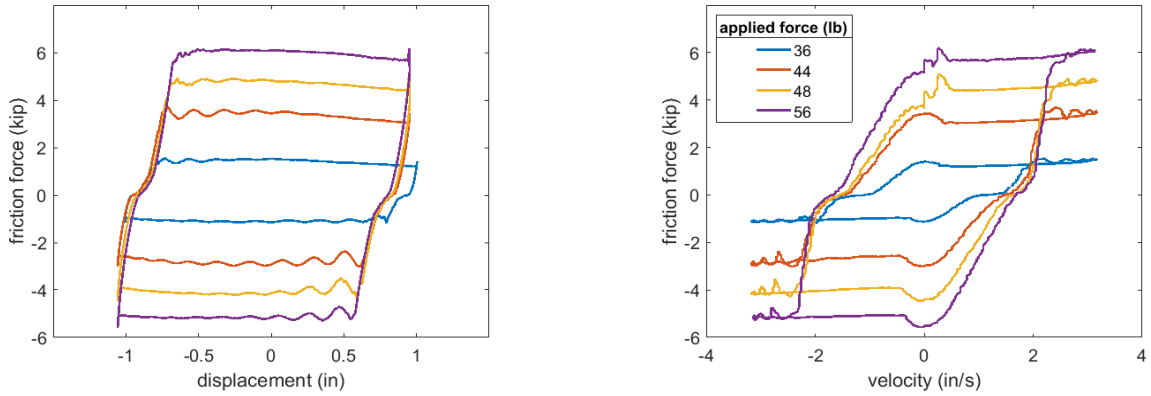

Fig. 4. Passive mode hysteresis loops for various applied forces: (a) force-displacement plots; (b) force-velocity plots.

It is noted that the standard LuGre model is unable to capture friction dynamics of the BRFD in regions of minimal damping. After the drum reaches peak displacement and reverses its direction

of travel, friction force quickly drops near zero as energy stored in the taut end of the bands is released. During this reversal, there is a short period where neither end of the bands are particularly taut, with little energy being stored in the system and the BRFD providing negligible damping. This effect – termed backlash by the authors – has previously been identified and addressed. Proposed has been a 3-stage dynamic friction model based on the standard LuGre model (Cao et al. 2015) as well as the real-time updating of LuGre model parameters using recurrent neural networks (Coble, Cao, Downey, Ricles 2023). For the purposes of this work, however, modeling backlash is not a concern as control inputs are only considered during periods of kinetic friction.

RELATIONSHIP DEVELOPMENT

To achieve semi-active control of the BRFD, it is necessary to understand the dependence of output friction on electric actuator displacements. To that end, an indirect, two-stage approach is adopted. Using data gathered from damper operation in passive mode, first the relationship between band tension (synonymous with electric actuator force) and damping is quantified. Analyzed next is the relationship between electric actuator positions and band tension. Considered together, the dependence of damping force on electric actuator displacements is indirectly identified.

Required first is passive mode characterization data detailing damper response to harmonic excitation. While datasets of this kind exist, they consist of inputs to the BRFD at various displacement amplitudes and frequencies (Coble, Cao, Ricles, Downey 2022). Being that damping depends on displacement amplitude, analysis of the relationship between damping force and electric actuator positions is easiest using a consistent input to the damper. As such, a single sinusoidal displacement profile is selected for repeated use in testing. An amplitude and frequency of 1in and 0.5Hz are chosen as they correspond to a moderate level of structural drift and a resonant frequency typical of taller buildings, respectively. At this point, suitable initial positions for the electric actuators are identified. These positions are such that (1) developed kinetic friction for forward and backward rotations is roughly equal and (2) accrued actuator forces are only a fraction of their maximum capacity. Beginning with the electric actuators at their initial positions, sets of passive characterization tests are conducted on three separate dates. Between tests, the positions

of the electric actuators are incrementally retracted until the force on either actuator exceeds a set safety limit during excitation. In total, data from 90 different characterization tests is collected.

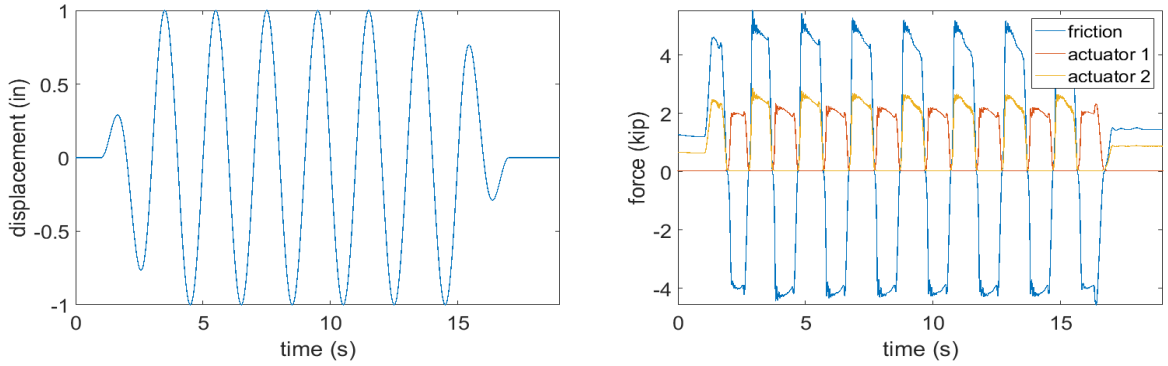

(a) **(b)**

Fig. 5. Example passive characterization data showing (a) displacement input and (b) damper response.

Displayed in Fig. 5 is an example of characterization input and the resulting response of the BRFD. Notice that as displacement increases, friction force is positive and only electric actuator two has an appreciable force on it. However, as displacement decreases, friction force is negative and only electric actuator one has an appreciable force on it. Fig. 6 shows the linear relationships that emerge when plotting friction force against electric actuator forces for both forward and backward rotations of the drum. While most clear when an actuator is taut, damping appears proportional to band tension even as an actuator is slack – at least for periods of above minimal damping. To recover damping force from the force on an electric actuator, then, an appropriate scaling factor may be used for forward and backward rotations of the drum. By fitting lines to all friction-actuator force plots generated from testing, scaling factors are taken as the slopes of the lines of best fit. The distribution of identified scaling factors is presented in Fig. 7. Intuitively, the scaling factors for both electric actuators while slack are not only much larger than those for while taut, but they also exhibit much greater variance. Because the force on a slack electric actuator is comparatively small, chatter constitutes a sizable fraction of the load cell signal. Consequently, regression parameters emerge highly variable.

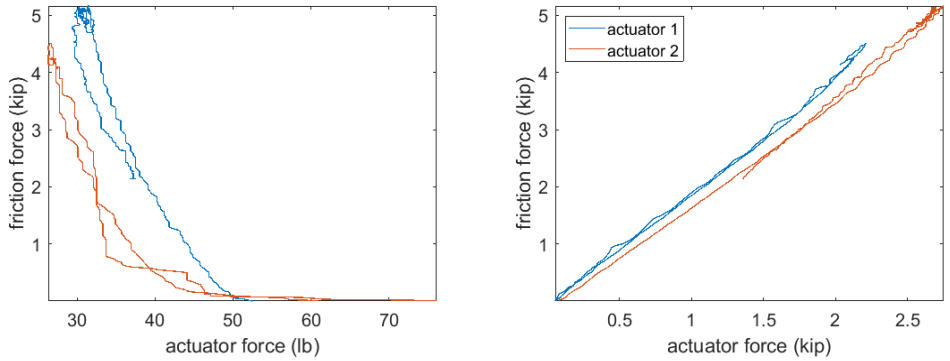

Fig. 6. Friction-actuator force dependence while electric actuators are (a) slack and (b) taut.

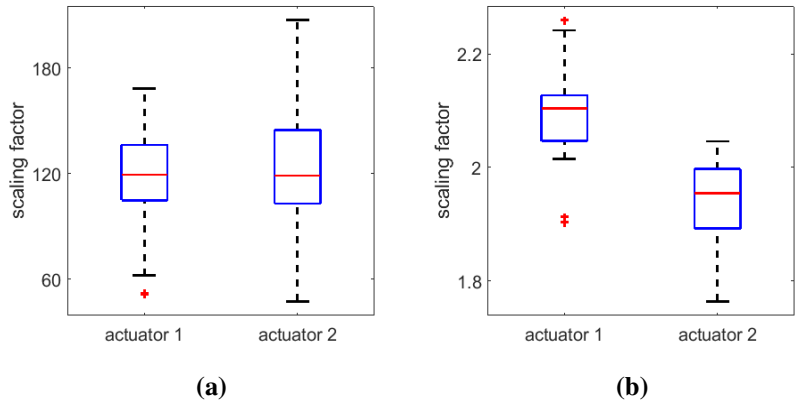

Fig. 7. Distribution of scaling factors for electric actuators while (a) slack and (b) taut.

For each set of characterization data, developed electric actuator forces during periods of kinetic friction are plotted against actuator initial positions. Performing multiple linear regression (MLR), models of the form $y = \beta_0 + \beta_1 x_1 + \beta_2 x_2 + \epsilon$ are fit to the data. Depicted in Fig. 8 are corresponding MLR models for one set of tests. Evident from this figure is that developed electric actuator forces are proportional to actuator positions. Interestingly, again this relationship appears to hold for actuators while both slack and taut. Because the BRFD is sensitive to setup conditions, regressing actuator forces against actuator initial positions is not for the purpose of expressing a direct relationship between the variables; such a dependence undoubtedly varies with slight altercations to the system anyway. Rather, MLR models seek to capture the rate at which

actuator forces vary with displacements of the electric actuators. Indeed, while the intercept terms of force-position models are inconsistent between sets of characterization data, the slope parameters appear regular.

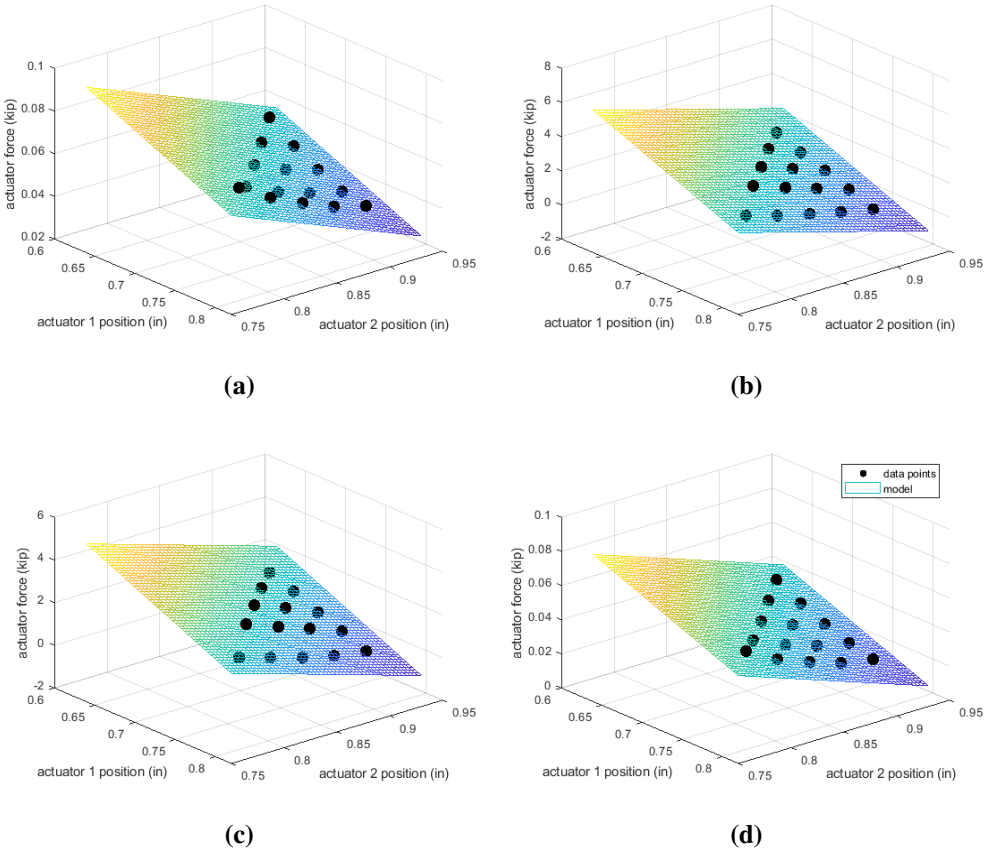

Fig. 8. Electric actuator force-position models for forward and backward rotations of the drum: (a) actuator 1 – slack; (b) actuator 2 – taut; (c) actuator 1 – taut; (d) actuator 2 – slack.

To further elucidate the viability of the BRFD for semi-active structural control, force amplification factors are computed from collected passive characterization data. These factors are the ratio of damping force to slack-actuator force during periods of kinetic friction. Hence, the BRFD has force amplification factors for both forward and backward rotations of the drum. Fig. 9 illustrates how these amplification factors are computed while Fig. 10 shows how they vary with applied forces to the electric actuators. Given its unique geometry, the BRFD is known to amplify applied forces more than that capable over a traditional, planar friction surface. Surprisingly, however, the

BRFD is able to achieve force amplification factors of at and above 200. Moreover, these factors clearly increase with applied tension in the elastic bands. The implication of aforementioned findings is that BRFD performance can be greatly enhanced via semi-active control; applied forces to the BRFD can not only be amplified tremendously, but the extent to which they are amplified may be controlled.

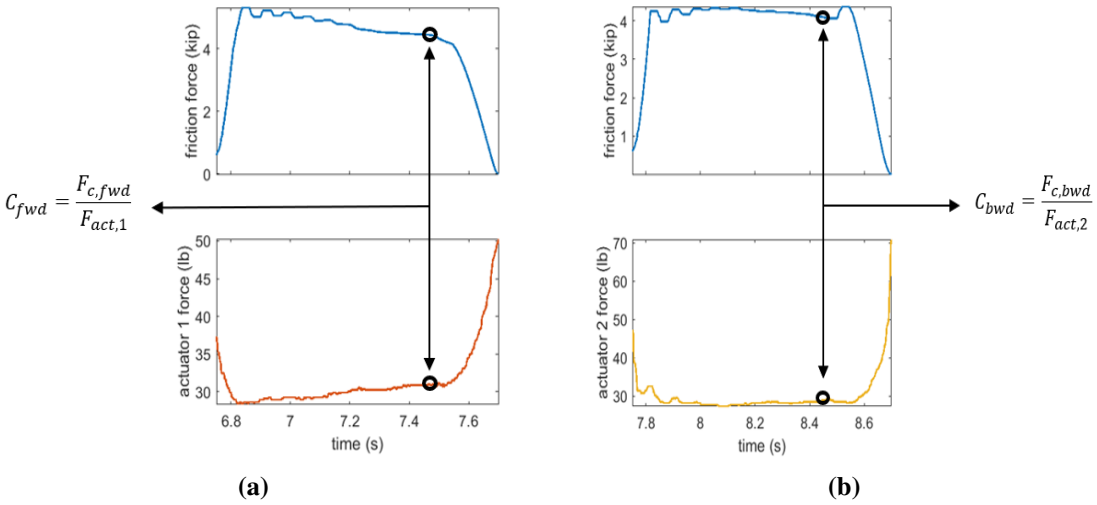

(a) **(b)**

Fig. 9. Visualization of force amplification factor computation: (a) forward rotations; (b) backward rotations.

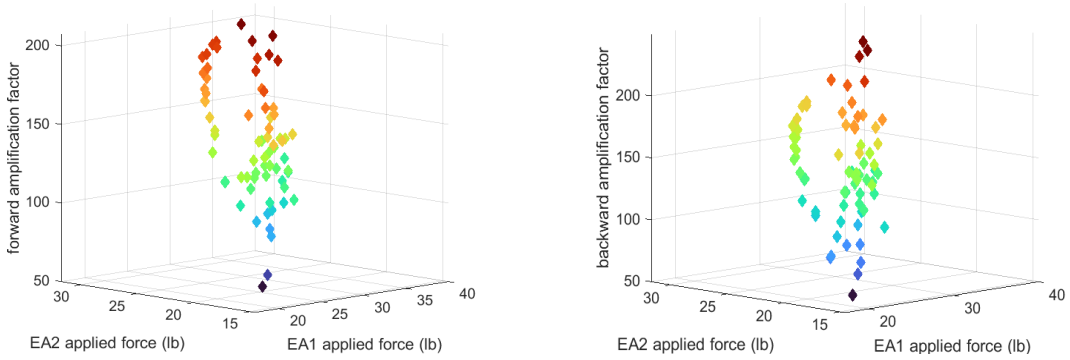

(a) **(b)**

Fig. 10. Dependence of damper amplification factors on applied electric actuator forces: (a) forward rotations; (b) backward rotations.

SEMI-ACTIVE MODEL

With knowledge of system dynamics in hand, now introduced is a semi-active model for the BRFD derived by letting developed kinetic friction be a function of electric actuator positions and drum velocity:

$$F_c(x_1, x_2, v) = \begin{cases} b + (C_1 m_{11} + C_2 m_{21})(x_1 - x_1') + (C_1 m_{12} + C_2 m_{22})(x_2 - x_2'), & v \geq 0 \\ b + (C_3 m_{31} + C_4 m_{41})(x_1 - x_1') + (C_3 m_{32} + C_4 m_{42})(x_2 - x_2'), & v < 0. \end{cases} \tag{4}$$

Here, x_1' and x_2' correspond to the initial positions of electric actuators one and two while x_1 and x_2 are the time-dependent positions of electric actuators one and two, respectively. v is simply the velocity of the drum. The m_{ij} slopes capture the rates at which electric actuator forces change with actuator displacements; they are identified as the average of the slopes obtained from force-position graphs like that in Fig. 8. C_1, C_2, C_3, and C_4 are the scaling factors allowing damping force to be approximated from the force an electric actuator. b is a constant kinetic friction value, that which develops with no actuator displacements from their initial positions. For erratic or asymmetric excitations, b itself may be a function of drum velocity, $b = \mathscr{F}(v)$. A summary of identified model slopes and scaling factors are given in Tables 1 and 2, respectively.

By design, the model assumes that the electric actuators act independently of each other and that changes in damping caused by simultaneous actuator displacements is simply the sum of the contributions of either actuator. This simplification, of course, ignores the potential for a coupling effect to exist between the electric actuators. Notice that if the actuators maintain position ($x_1 = x_1'$ and $x_2 = x_2'$) for the entire duration of excitation, $F_c(x_1, x_2, v)$ reduces to a constant. Furthermore, because all slopes are negative, if either electric actuator retracts while slack or taut (x_1 or x_2 decreases), kinetic friction and consequently damping increases. The opposite is true for electric actuator extension (x_1 or x_2 increases). Substitution of the derived kinetic friction function into Eq. 2 gives

$$g(v) = F_c(x_1, x_2, v) + (F_s - F_c(x_1, x_2, v))e^{-(v/v_s)^2}, \tag{5}$$

a small modification to the standard LuGre model allowing for changes in damper output during periods of kinetic friction to be predicted from electric actuator displacements.

Table 1. Identified model slopes

	Slope (kip/in)							
	m_{11}	m_{12}	m_{21}	m_{22}	m_{31}	m_{32}	m_{41}	m_{42}
Value	-0.14	-0.15	-15.29	-13.00	-16.66	-15.77	-0.13	-0.15

Table 2. Identified model scaling factors

	Scaling Factor			
	C_1	C_2	C_3	C_4
Value	119.68	2.10	1.94	123.31

VALIDATION

To validate the proposed dynamic model, semi-active validation tests are devised that run hydraulic and electric actuators simultaneously. Drum displacement is provided by a harmonic input to the MTS hydraulic actuator with amplitude 1in and frequency 0.5Hz. As with previous characterization tests, the input sinusoid ramps up and down to start and end the test. For select cycles of drum rotation, the electric actuators are commanded to retract and extend following a displacement input from their initial positions. In total, 12 validation tests are conducted, six with harmonic electric actuator displacements and six with step electric actuator displacements. Descriptions of conducted validation tests are provided in Table 3.

Table 3. Electric actuator displacement parameters for both harmonic and step validation tests

Test #	**Controlled Actuator**	**Displacement Amplitude (in)**	**Drum Rotation**
1	one	0.03	forward
2	one	0.03	backward
3	two	0.03	forward
4	two	0.03	backward
5	both	0.015	forward
6	both	0.015	backward

Using measured responses of the electric actuators, semi-active model predictions are made for all validation tests; Table 4 details model normalized root mean squared error (NRMSE) on the validation dataset. Figs. 11 and 12 show semi-active profiles along with associated damper output and model predictions for a harmonic and step-type validation test, respectively. Notice the dynamic kinetic friction values that result from electric actuator displacements. Fig. 13 displays force-velocity plots along with semi-active model predictions for those validation profiles in Figs. 11 (a) and 12 (a).

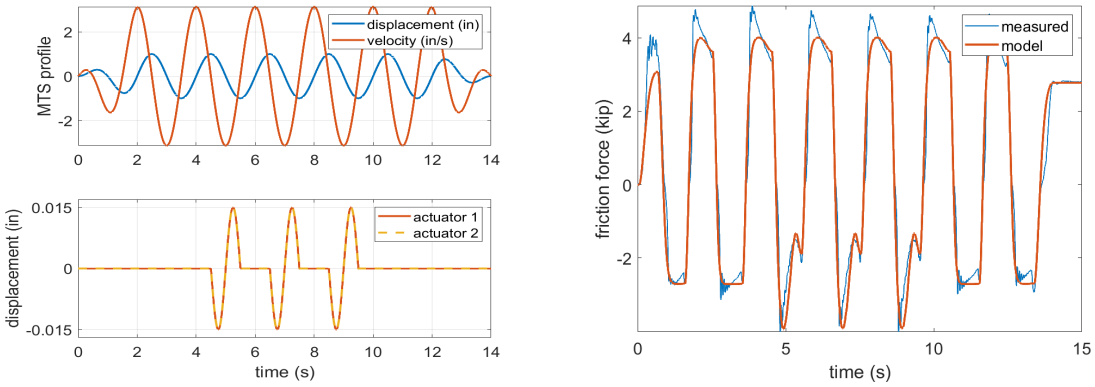

(a) **(b)**

Fig. 11. Harmonic validation test 6 data showing (a) displacement inputs and (b) damper response with model predictions.

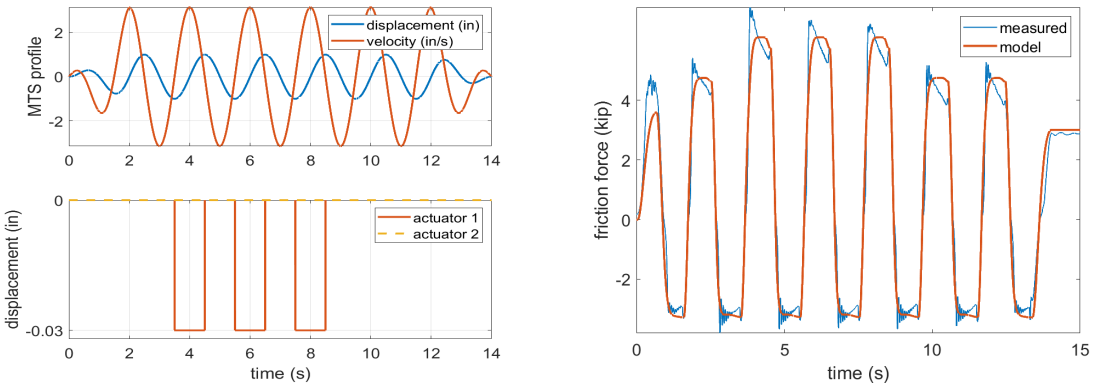

(a) **(b)**

Fig. 12. Step validation test 3 data showing (a) displacement inputs and (b) damper response with model predictions.

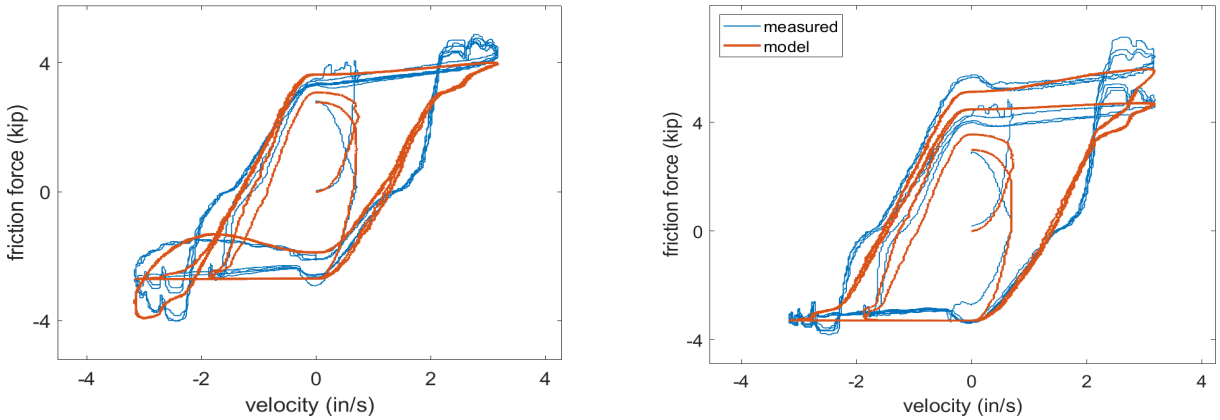

Fig. 13. Hysteresis plots and semi-active model predictions for (a) harmonic validation test 6 and (b) step validation test 3.

Table 4. Model error summary

	NRMSE	
Test #	Harmonic	Step
1	0.1988	0.1766
2	0.2070	0.1794
3	0.1971	0.1684
4	0.1939	0.1792
5	0.1984	0.1768
6	0.1908	0.1717

DISCUSSION

Given its dynamic kinetic friction parameter, the semi-active model successfully captures changes in damping induced by electric actuator displacements. While the model does exhibit appreciable error on the validation dataset, much of this error stems from difficulties in fitting LuGre model parameters and an inability to replicate the backlash effect. Furthermore, discrepancies often arise between initial model predictions and measured friction as residual static force can persist between the drum and elastic bands following excitation. See Fig. 14 for a visualization of described model error modes.

Compared to those drum cycles with no displacements of the electric actuators, semi-active tests achieved on average a 33% increase in damper amplification factors for both forward and backward rotations of the drum. Realizing this level of amplification increase is compelling, especially considering that displacement inputs to the electric actuators were at most 0.03in for validation tests. By next investigating limitations of electric actuator response times, the scope of BRFD semi-active control can be quantified.

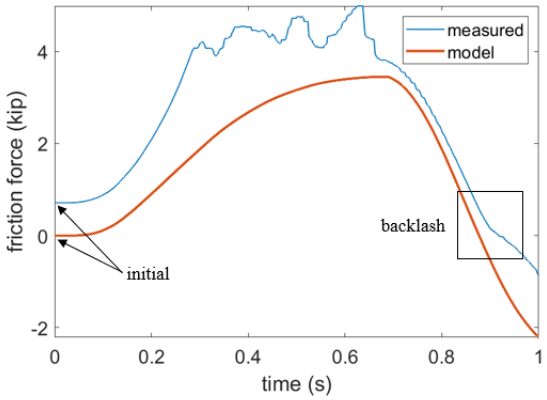

Fig. 14. Model error arising from initial prediction discrepancy and backlash.

SUMMARY AND CONCLUSIONS

This work sought to develop a model for semi-active control of a rotary friction damper whereby developed kinetic friction is controlled via displacement inputs to electric actuators. Using data collected from damper operation in passive mode, the relationship between damper output and electric actuator displacements was identified. By deriving a dynamic F_c parameter, a corresponding semi-active model based on the LuGre dry friction model was proposed. Altogether, with the relationship between electric actuator displacements and kinetic friction now understood, future work may proceed with the development of semi-active control algorithms for internal control of the BRFD. This includes eventual hybrid simulations of the controlled BRFD installed within a structure for multihazard mitigation.

ACKNOWLEDGMENTS

This material is based upon work supported by the National Science Foundation under the NHERI Network Coordination Grant No. 2129782 and the Lehigh University, Real-Time Multi-Directional Hybrid Simulation Experimental Facility Grant No. 2037771. Discussed findings are those of the authors and do not necessarily reflect the view of the National Science Foundation. The authors wish to thank Lehigh University, the Lehigh NHERI Experimental Facility, and the ATLSS Engineering Research Center for hosting this work. Much appreciated are Thomas Marullo and laboratory maintenance technicians for help with damper testing and troubleshooting, respectively. Extended thanks go out to Drs. Robin Nelson, Chad Kusko, and Joseph Saunders for their work in organizing the NHERI REU and STEM-SI summer programs. Without their help, this work would not have been possible.

REFERENCES

Agrawal A. K. and J. Yang. 2004. "A semi-active electromagnetic friction damper for response control of structures." In *Proc., Structures Congress 2000*, 1-8. Philadelphia: Structural Engineering Institute of ASCE. https://doi.org/10.1061/40492(2000)6.

Canudas de Wit, C., H. Olsson, K. J. Astrom, and P. Lischinsky. 1995. "A new model for control systems with friction." *IEEE Trans. Autom. Control.* 40 (3), 419-425. https://doi.org/10.1109/9.376053.

Cao, L., A. Downey, S. Laflamme, D. Taylor, and J. Ricles. 2015. "Variable friction device for structural control based on duo-servo vehicle brake: Modeling and experimental validation." *J. Sound. Vib.* 348, 41-56. https://doi.org/10.1016/j.jsv.2015.03.011.

Cao, L., S. Laflamme, D. Taylor, and J. Ricles. 2016. "Simulations of a variable friction device for multihazard mitigation." *J. Struct. Eng.* 142 (12), H4016001. https://doi.org/10.1061/(ASCE)ST.1943-541X.0001580.

Coble, D., L. Cao, A. Downey, and J. Ricles. 2023. "Deep-learning-based friction modeling of dry interfaces for structural dampers." In *Proc., IMAC 41*, 1-7. Austin: Society for Experimental Mechanics. https://doi.org/10.1007/978-3-031-36663-5_27.

Coble, D., L. Cao, J. Ricles, and A. Downey. 2022. "Dataset-friction-damper-with-backlash." https://github.com/ARTS-Laboratory/Dataset-Friction-Damper-with-Backlash.

Downey, A., L. Cao, S. Laflamme, D. Taylor, and J. Ricles. 2016. "High capacity variable friction damper based on band break technology." *Eng. Struct.* 113, 287-298. https://doi.org/10.1016/j.engstruct.2016.01.035.

Dupont, P., P. Kasturi, and A. Stokes. 1997. "Semi-active control of friction dampers." *J. Sound. Vib.* 202 (2), 203-218. https://doi.org/10.1006/jsvi.1996.0798.

dos Santos, M. B., H. T. Coelho, F. P. L. Neto, and J. Mahfoud. 2017. "Assessment of semi-active friction dampers." *Mech. Syst. Signal Process.* 94, 33-56. https://doi.org/10.1016/j.ymssp.2017.02.034.

Elias, S. and V. Matsagar. 2017. "Research developments in vibration control of structures using passive tuned mass dampers." *Annu. Rev. Control.* 44, 129-156. https://doi.org/10.1016/j.arcontrol.2017.09.015.

Johanastrom, K. and C. Canudas de Wit. 2008. "Revisiting the LuGre friction model." *IEEE Control Syst. Mag.* 28 (6), 101-114. https://doi.org/10.1109/MCS.2008.929425.

Lu, L.-Y. 2004. "Semi-active modal control for seismic structures with variable friction dampers." *Eng. Struct.* 26 (4), 437-454. https://doi.org/10.1016/j.engstruct.2003.10.012.

Lu, L.-Y., T.-K. Lin, R.-J. Jheng, and H.-H. Wu. 2018. "Theoretical and experimental investigation of position-controlled semi-active friction damper for seismic structures." *J. Sound. Vib.* 412, 184-206. https://doi.org/10.1016/j.jsv.2017.09.029.

Pinkaew, T. and Y. Fujino. 2001. "Effectiveness of semi-active tuned mass dampers under harmonic excitation." *Eng. Struct.* 23 (7), 850-856. https://doi.org/10.1016/j.engstruct.2003.10.012

Rahimi, F., R. Aghayari, and B. Samali. 2020. "Application of tuned mass dampers for structural vibration control: a State-of-the-art review." *Civ. Eng. J.* 1622-1651. https://doi.org/10.28991/cej-2020-03091571.

Saaed, T. E., G. Nikolakopoulos, J.-E. Jonasson, and H. Hedlun. 2015. "A State-of-the-art review

of structural control systems." *J. Vib. Control.* 21 (5), 919-937. https://doi.org/10.1177/1077546313478294.